Journal of Physics: Conference Series **3224** (2026) 042021 doi:10.1088/1742-6596/3224/4/042021

Implicit large eddy simulations for the actuator line method of wind turbine

Guiyu Cao[1,2,3], Christopher Vogel[1], Markella Zormpa[1] and Qibing Li[2]

[1]Department of Engineering Science, University of Oxford, Oxford, UK
[2]Department of Engineering Mechanics, Tsinghua University, Beijing, China
[3] SuStream Energy Technology Co., Ltd., Suzhou, Jiangsu Province, China

E-mail: christopher.vogel@eng.ox.ac.uk

Abstract. This paper evaluates the effects of the Sub-grid Stress (SGS) model on wind turbine simulations using the Actuator Line Method (ALM), taking into account numerical discretisation error, SGS modelling error and blade modelling error. The investigation covers the implicit Large Eddy Simulation (iLES) model, the Wall-adapting Local Eddy-viscosity (WALE) model, and the Smagorinsky model (SM). A detailed analysis of the aerodynamic loads and wake behaviour of the NTNU benchmarking turbine Blind Test 1 is conducted, with uniform laminar and turbulent inlets imposed at varying grid resolutions, both with and without nacelle geometry. A turbulent inlet triggers an earlier transition and results in faster wake recovery. The explicit SGS model is not necessary for predicting total power coefficients and aerodynamic loadings as blade modelling errors are qualitatively dominant. Under a turbulent inlet, the time-averaged velocity is insensitive to SGS models on both coarse and fine grids. For resolved turbulent kinetic energy, the WALE model with a coarse grid provides slightly better resolution than the iLES and SM models in the far wake region. In conclusion, iLES is workable for the ALM of wind turbines.

1. Introduction

The Actuator Line Method (ALM) [1] has become a widely used mid-fidelity alternative to expensive blade-resolved simulations for predicting aerodynamic loads and wind turbine wakes [2]. In the ALM, an explicit Large Eddy Simulation (eLES) using an explicit Subgrid-scale (SGS) model is usually taken granted to simulate the unsteady turbulent wakes under unresolved grids.

Zero-equation eddy viscosity models are by far the most commonly used class of eLES models, e.g., the Smagorinsky model (SM) proposed by Manabe et al. [3]. SM models unresolved turbulent structures through a gradient-type assumption between the SGS stress and the resolved velocity gradient. In practice, SM requires to adjust empirical coefficient according to the flow types. In this two decades, modified zero-equation eddy-viscosity models have been developed to be comparable with dynamic SM while still keep the simple algebraic form, such as Wall-adapting Local Eddy-viscosity (WALE) model [4], Vreman-type model [5].

Different with the explicit SGS model in eLES, the implicit Large Eddy Simulation (iLES) takes the built-in numerical dissipation as the SGS dissipation, and does not require an explicit SGS model [6, 7]. Recent work [8] has evaluated quantitative comparisons on the modelling SGS dissipation rate in eLES and numerical SGS dissipation rate in iLES. The explicit modelling SGS dissipation in eLES pollutes the resolved turbulent structures in benchmarking Taylor-Green

vortex turbulence. Due to the lower computational costs and reasonable performance, iLES has gradually been utilized in wind turbine wakes simulations [9, 10].

ALM is much more efficient than blade-resolved simulations in wind turbines, as each rotor blade is represented by a spanwise distribution of actuator points. These points form a line that rotates to mimic the effect of the blades, eliminating the need for direct meshing. The ALM consists of three key steps: velocity sampling, force calculation, and force smearing in the flow [2]. There exist the inherent blade modelling error in the ALM. For instance, it is best to decrease the smearing kernel size as much as possible. The lower limit is typically given by the numerical stability of the solver.

To the author's knowledge, there is no determined empirical modelling coefficients in eLES models for wind turbine wake simulation. Given the inherent errors in numerical discretisation and blade modelling in the ALM, this work presents an evaluation of iLES for benchmarking wind turbine [11], alongside comparisons of zero-equation eddy viscosity models: SM and WALE model. The detailed analysis of aerodynamic loads and wake behaviour are implemented under the uniform laminar and turbulent inlets with varying grid resolution and smearing kernel size, with and without nacelle geometry.

In the following, components of the total numerical error are analyzed in Section 2. Section 3 presents the numerical setups for benchmarking turbine. Section 4 discusses the large eddy simulations for the ALM of wind turbines. The summary of findings is presented in Section 5.

2. Components of the total numerical error

For the physical quantity of interest, $\phi(\boldsymbol{x})$, in the wind turbine simulation, the numerical value obtained by the ALM using the SGS model reads $\phi^{num}(\boldsymbol{x})$. Here, we focus on the time-averaged statistical quantity of interest. We define the total numerical error $\epsilon^{num}(\boldsymbol{x})$ as

$$\phi(\boldsymbol{x}) \equiv \phi^{num}(\boldsymbol{x}) + \epsilon^{num}(\boldsymbol{x}), \quad \epsilon^{num}(\boldsymbol{x}) = \epsilon^{n}(\boldsymbol{x}) + \epsilon^{t}(\boldsymbol{x}) + \epsilon^{b}(\boldsymbol{x}). \tag{1}$$

In Eq (1), $\epsilon^{n}(\boldsymbol{x})$ denotes the numerical discretisation error, $\epsilon^{t}(\boldsymbol{x})$ the SGS modelling error, and $\epsilon^{b}(\boldsymbol{x})$ the blade modelling error.

The numerical discretisation error, $\epsilon^{n}(\boldsymbol{x})$, mainly arises from the inherent numerical dissipation and numerical dispersion, both of which are determined by the numerical scheme. The SGS modelling error $\epsilon^{t}(\boldsymbol{x})$ is inevitable when introducing the SGS model to achieve the expected solution while reducing the computational costs under unresolved grids. In ALM, we use the discrete actuator points to represent the 3D blade, which introduces a blade modelling error, denoted by $\epsilon^{b}(\boldsymbol{x})$. Since the numerical dissipation in iLES acts as the SGS dissipation, the total numerical error only contains $\epsilon^{n}(\boldsymbol{x})$ and $\epsilon^{b}(\boldsymbol{x})$ in iLES.

The numerical discretisation error $\epsilon^{n}(\boldsymbol{x})$ is fixed to the order of $\max\{\mathcal{O}(\Delta x)^2, \mathcal{O}(\Delta t)^2\}$ in the current simulations, since the second-order centered spatial and second-order backward temporal discretisation schemes are used in the OpenFOAM-v2312. Here, Δx is the grid size and Δt is the time step in the numerical discretisation. According to the CFL condition, Δt is smaller than Δx, so the numerical discretisation error is dominated by the grid size Δx. The SGS modelling error $\epsilon^{t}(\boldsymbol{x})$ varies with the iLES, and the SM and the WALE model. In current simulations, the defaulted SGS model coefficients are used in the OpenFOAM. The in-house ALM [2] has been well developed. In ALM, the the blade modelling error $\epsilon^{b}(\boldsymbol{x})$ varies with the empirical spherical Gaussian kernel size ε in $2\Delta x$ and $3\Delta x$. We adopt 100 actuator points in the following simulations.

3. Numerical setups

We simulate the NTNU rotor designed for Blind Test 1 (BT1) [11], which is three-bladed, with a diameter of $D = 0.894$ meters and a height of the hub center $H = 0.8$ meters. The design

tip-speed ratio is $\lambda = 6$, and the freestream velocity is $U_\infty = 10m/s$. The chord-based Reynolds number defined as $Re_c = cV_{rel}/\nu$, where c the chord length, V_{rel} the relative velocity incident to the blade section and ν the kinematic viscosity, is here $Re_c = 10^5$ at the tip.

The computational domain takes $(x, y, z) \in (-4D, 14D) \times (-1.5D, 1.5D) \times (0D, 2D)$, where x-, y- and z- denotes streamwise, lateral and vertical directions, respectively. The center of the turbine is located at $(0D, 0D, 1H)$. The computational domain employs two main refinement levels: an outer coarser region and an inner finer region. The inner region spans the coordinates $(-0.5D, 9.5D) \times (-0.75D, 0.75D) \times (0D, 1.7D)$, and uniform grid resolutions of $D/50$ and $D/100$ are currently in use in the inner finer region. The wind tunnel of the BT1 is modeled using a symmetry boundary condition on the walls. The inlet has a uniform fixed velocity of $U_\infty = 10m/s$ and the outlet has a zero pressure gradient.

Table 1. Numerical setups for the ALM. The grid size is set in the inner finer region. The default smearing kernel size is $2\Delta x$.

Cases	Laminar inlet	Turbulent inlet	Turbulent inlet with nacelle
Coarse grid ($\Delta x = D/50$)	$L1$	$T1$	T_N1
Fine grid ($\Delta x = D/100$)	$L2$	$T2$	T_N2

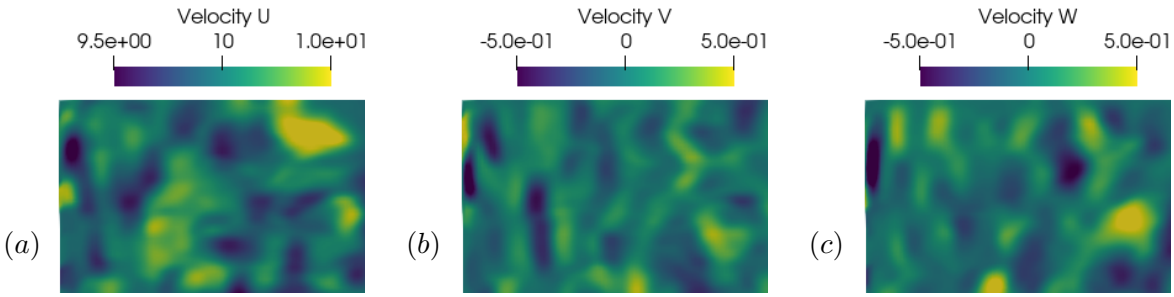

Figure 1. Instantaneous velocity contours upstream the wind turbine at $y = 0D$ for $T2$ cases. U, V and W represent the streamwise, lateral and vertical velocity, respectively.

Table 1 shows the numerical setups for a uniform laminar inlet (cases $L1$ and $L2$) and a turbulent inlet varying grid resolution, without nacelle (cases $T1$ and $T2$) and with nacelle geometry (cases $TN1$ and $TN2$). For the turbulent inlet, the synthetic eddies are superimposed at the inlet using the divergence free synthetic eddy method (DFSEM) [12]. The initial integral length scale is set to 0.3 meters at $x = -4D$. After free decay, the turbulence intensity (TI) at the hub center of $2D$ upstream of the wind turbine is controlled to approximately $TI = 1.8\%$. Figure 1 illustrates the instantaneous velocity contours generated by the DFSEM upstream of the wind turbine. For the turbulent inlet with nacelle cases, the nacelle is modeled using the cell-blocking method [13]. In ALM, the default smearing kernel size is $2\Delta x$, and a wider smearing kernel size of $3\Delta x$ is also implemented to investigate the blade modelling error.

4. Actuator line simulations of wind turbine

4.1. Effect of laminar and turbulent inlets

Figure 2 illustrates the instantaneous fully-developed wakes for the $L1$ cases varying SGS models under a laminar inlet, the magnitude of vorticity is 50. The wakes from the iLES and WALE models are qualitatively similar, whereas the SM provides a longer wake similar to the iLES with a larger smearing kernel size $3\Delta x$, indicating a slower wake recovery. Qualitatively, the performance of the wakes is sensitive to the SGS models for a uniform laminar inlet.

Figure 3 illustrates the instantaneous fully-developed wakes for the $T2$ cases varying SGS models under the turbulent inlet, the magnitude of vorticity is 50. The wakes are all qualitatively

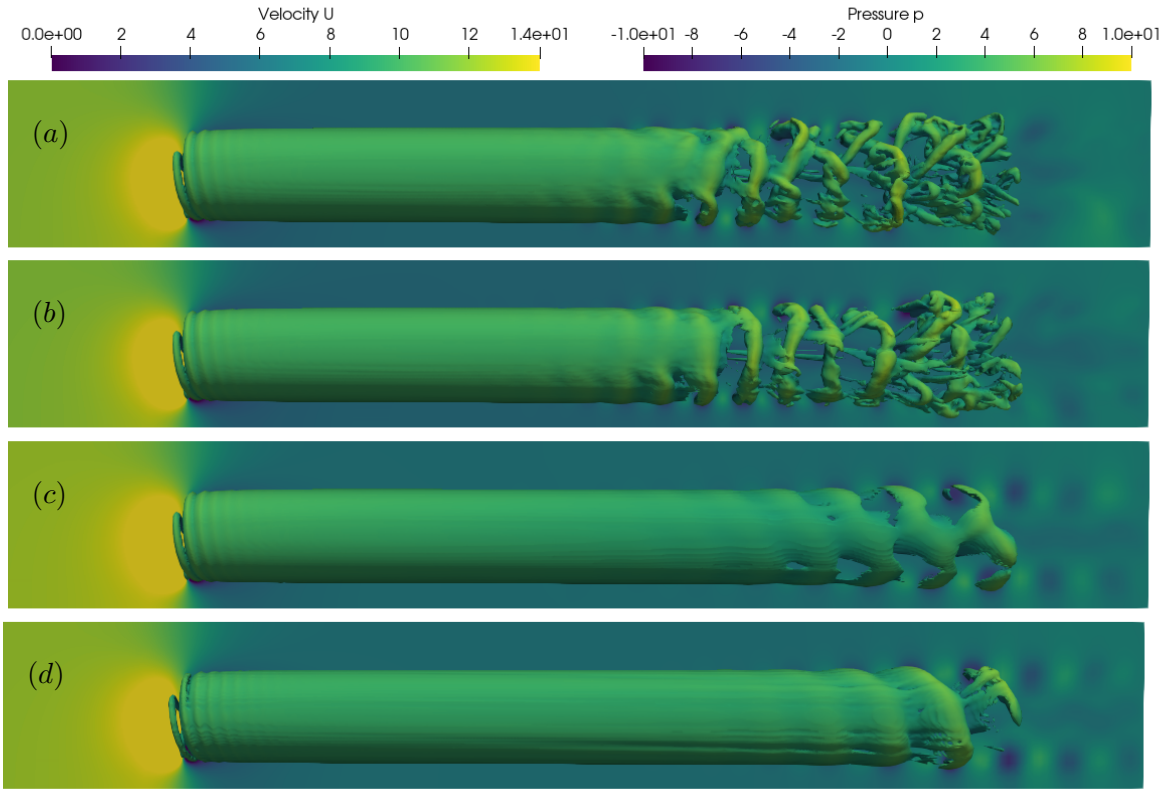

Figure 2. Instantaneous vorticity contours colored by streamwise velocity, and pressure contours are at $y = 0D$ for $L1$ cases: iLES (a), WALE (b), SM (c), and iLES with $\varepsilon = 3\Delta x$ (d).

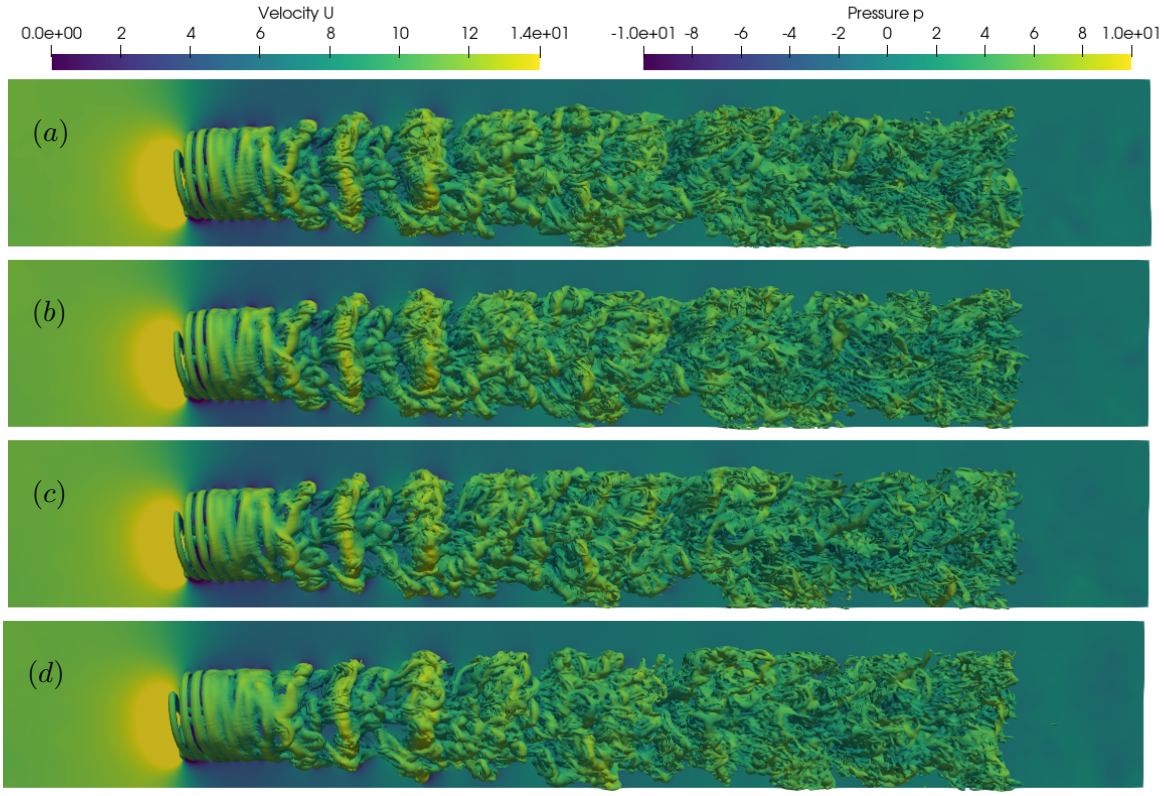

Figure 3. Instantaneous vorticity contours colored by streamwise velocity, and pressure contours are at $y = 0D$ for $T2$ cases: iLES (a), WALE (b), SM (c), and iLES with $\varepsilon = 3\Delta x$ (d).

similar and show an earlier transition and vortex breakdown compared to those under the laminar inlet shown in Figure 2. The turbulent inlet triggers an earlier transition and a faster wake recovery. For a turbulent inlet, wakes performance is qualitatively insensitive to the SGS models.

4.2. Total power coefficient and loading forces

Figure 4 presents the history of the total power coefficient, C_p, where the initial time is set to $100T$ in order to bypass the initial transient period. T is the time period for the blade to complete one revolution. For the coarse grid, the total power coefficient is insensitive to the SGS models and the smearing kernel size. Under a laminar inlet, the fluctuations in C_p are very small, whereas the turbulent inlet causes larger fluctuations in C_p. For the fine grid, the total power coefficient is insensitive to the SGS models, but depends on the smearing kernel size. This indicates that the blade modelling error, $\epsilon^b(\boldsymbol{x})$, qualitatively dominates. These observations also apply to the thrust coefficient, which is ignored here.

Figure 5 presents the time-averaged tangential force. For the coarse grid, the tangential force is insensitive to the SGS models and the size of the smearing kernel. For the fine grid, however, the tangential force depends on the smearing kernel size, while being insensitive to the SGS models. These observations are consistent with the findings for the total power coefficient. Figure 6 presents the variation of tangential force from $100T$ to $140T$. With the same grid resolution and SGS model, the turbulent inlet causes a larger variation than that under the uniform laminar inlet. In addition, the fine grid provides the relatively larger variation than the coarse grid, indicating that the numerical discretisation error $\epsilon^n(\boldsymbol{x})$ qualitatively dominates. These observations also hold for the axial force ignored here.

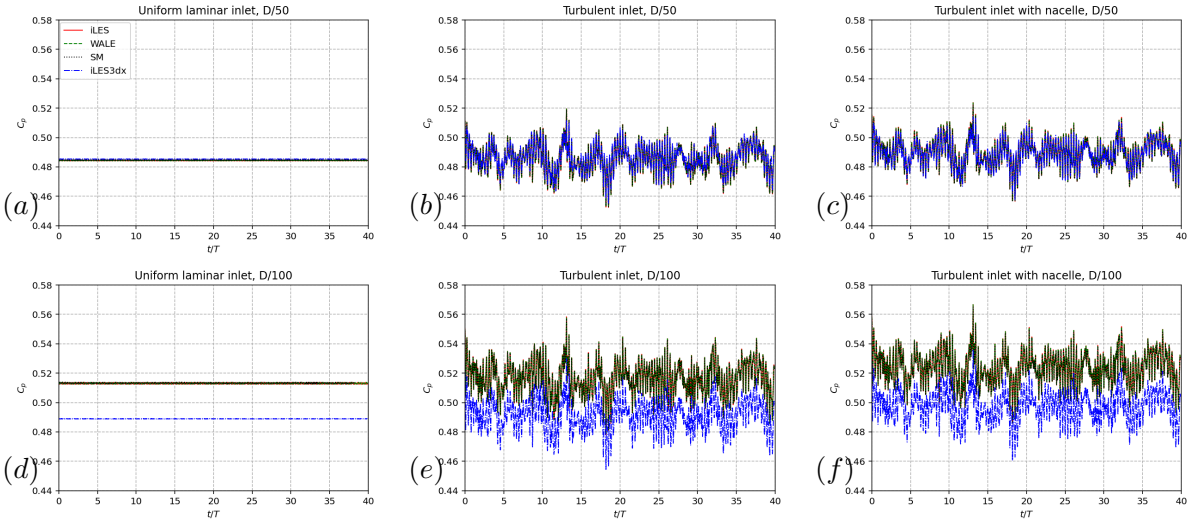

Figure 4. The history of total power coefficient Cp profiles under the uniform laminar (a) (d), the turbulent inlets (b) (e), and the turbulent inlets with nacelle (c) (f). The upper row is for coarse grid, and the bottom row is for fine grid.

4.3. Turbine wake analysis

4.3.1. Near-wake region Figure 7 presents the time-averaged velocity profiles downstream $1D$ wind turbine at $z = 1H$. For both the coarse and fine grids, the velocity profile is insensitive to the SGS models, but depends on the smearing kernel size. This indicates that the blade

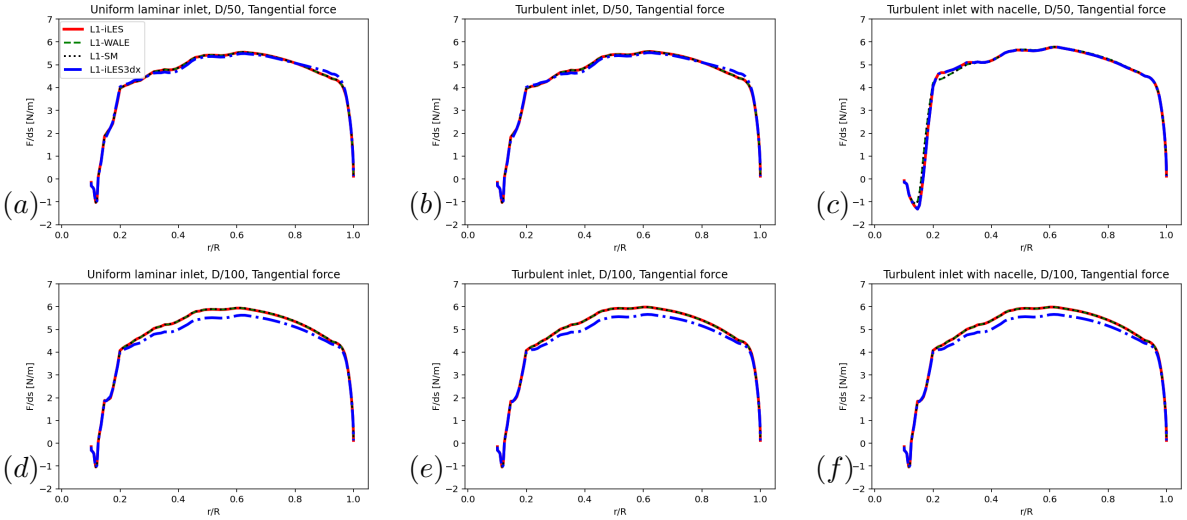

Figure 5. Time-averaged tangential force profiles under the uniform laminar (a) (d), the turbulent inlets (b) (e), and the turbulent inlets with nacelle (c) (f). The upper row is for coarse grid, and the bottom row is for fine grid.

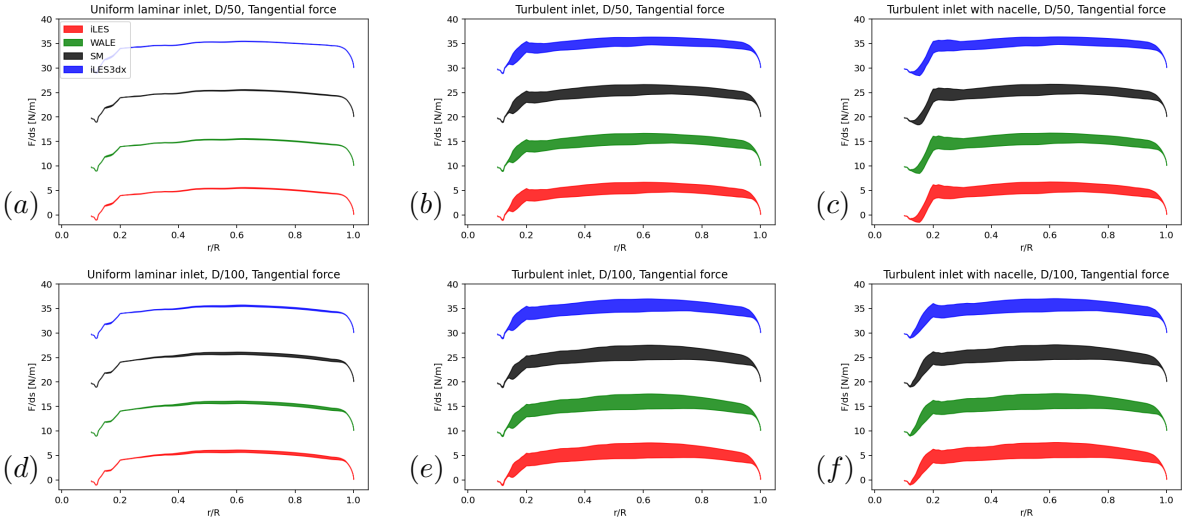

Figure 6. Variations of tangential force profiles under the uniform laminar (a) (d), the turbulent inlets (b) (e), and the turbulent inlets with nacelle (c) (f). The upper row is for coarse grid, and the bottom row is for fine grid. The force profiles shift by 10 units along the vertical axis with each increment from the bottom line.

modelling error, $\epsilon^b(\boldsymbol{x})$, qualitatively dominates. In the T_N1 case, the nacelle modeled using the cell-blocking method causes greater velocity deceleration.

Figure 8 presents the time-averaged resolved Turbulent Kinetic Energy (TKE) profiles downstream $1D$ wind turbine at $z = 1H$. For the coarse grid, the iLES and SM models provide larger resolved TKE, especially in the tip-vortex region. In contrast, the WALE model and the iLES model with $\varepsilon = 3\Delta x$ provide smaller resolved TKE. In the tip-vortex region, WALE model almost can not resolve TKE. These observations also apply to the fine grid, except that the WALE model produces the highest resolved TKE values in the hub-vortex region with the nacelle. In the tip-vortex region, the smaller TKE is resolved in the $T2$ and T_N2 cases with

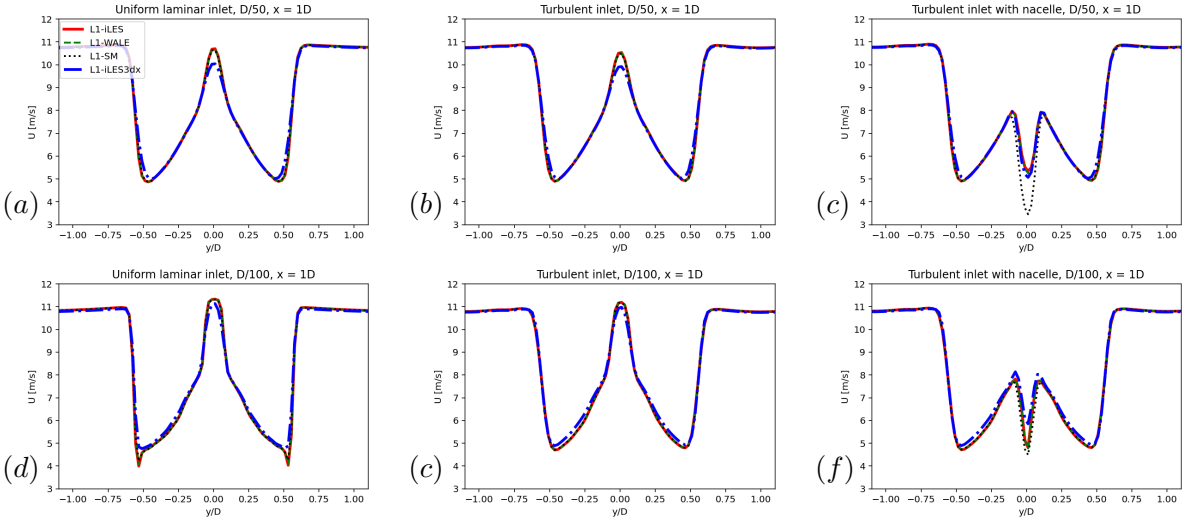

Figure 7. Time-averaged velocity profiles downstream $1D$ wind turbine at $z = 1H$ under the uniform laminar (a) (d), the turbulent inlets (b) (e), and the turbulent inlets with nacelle (c) (f). The upper row is for coarse grid, and the bottom row is for fine grid.

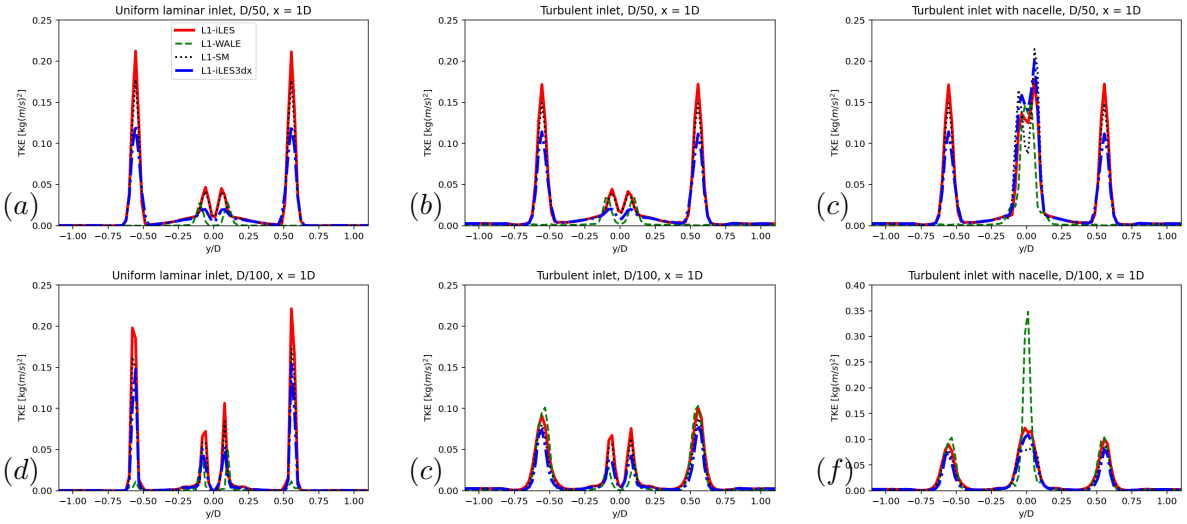

Figure 8. Time-averaged resolved TKE profiles downstream $1D$ wind turbine at $z = 1H$ under the uniform laminar (a) (d), the turbulent inlets (b) (e), and the turbulent inlets with nacelle (c) (f). The upper row is for coarse grid, and the bottom row is for fine grid.

the fine grid than in the $T1$ and T_N1 cases with the coarse grid. In summary, the numerical discretisation error $\epsilon^n(\boldsymbol{x})$ and the SGS modelling error $\epsilon^t(\boldsymbol{x})$ qualitatively dominate the resolved TKE performance in the near-wake region.

Figure 9 presents the Power Spectral Density (PSD) of stream velocity at the $(1D, 0, 1H + 1/2D)$. For the uniform laminar inlet cases, L_1 and L_2, we observe a spike in the PSD at the Blade Passing Frequency (BPF), f_B. However, the turbulent inlet triggers the breakdown of the tip vortex earlier, and no BPF spike is observed. In case $L2$, the spike at $2f_B$ shows the harmonic performance of the near-wake flow structure. In the low-frequency region ($f \leq 1f_B$), the iLES, SM and WALE models all provide a similar PSD, with solution from the iLES deviating due

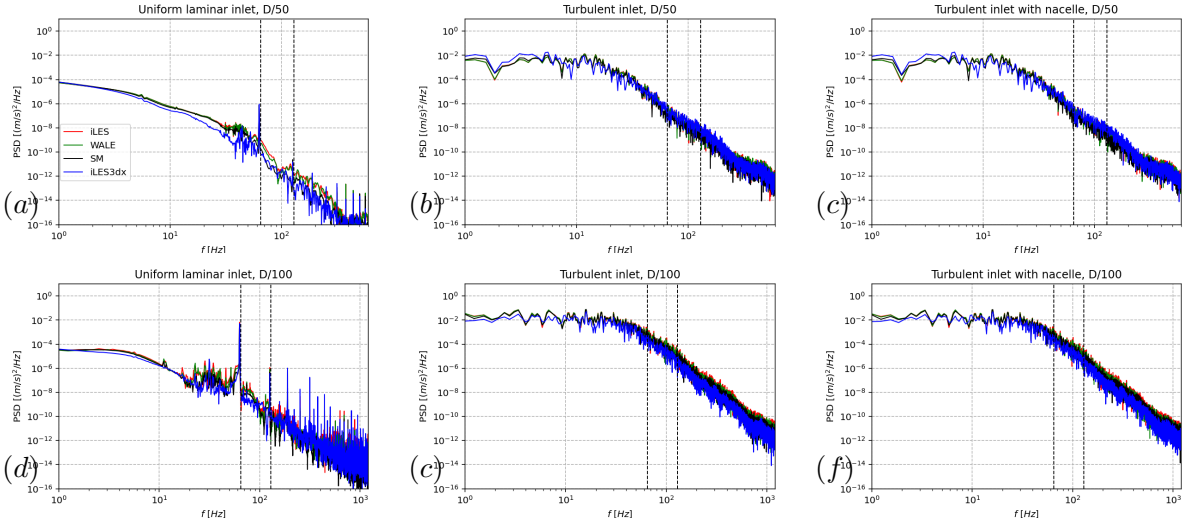

Figure 9. PSD of streamwise velocity at the $(1D, 0, 1H + 1/2D)$ under the uniform laminar (a) (d), the turbulent inlets (b) (e), and the turbulent inlets with nacelle (c) (f). The upper row is for coarse grid, and the bottom row is for fine grid. Two vertical dashed lines are at f_B and $2f_B$.

to its wider smearing kernel size. In summary, the blade modelling error, $\epsilon^b(\boldsymbol{x})$, qualitatively dominates the PSD performance.

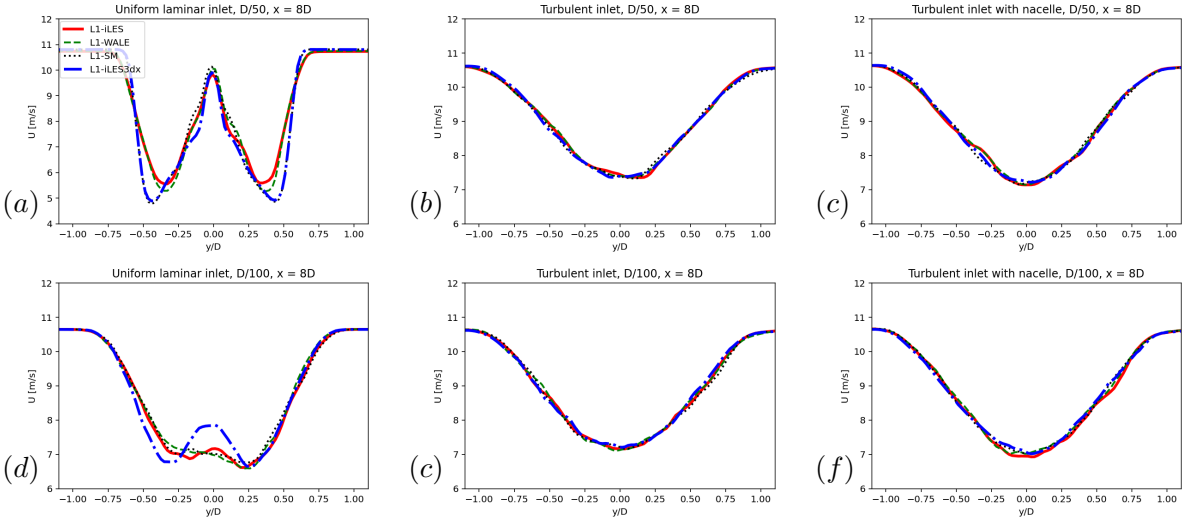

Figure 10. Time-averaged velocity profiles downstream $8D$ wind turbine at $z = 1H$ under the uniform laminar (a) (d), the turbulent inlets (b) (e), and the turbulent inlets with nacelle (c) (f). The upper row is for coarse grid, and the bottom row is for fine grid.

4.3.2. Far-wake region Figure 10 presents the time-averaged velocity profiles downstream $8D$ wind turbine at $z = 1H$. For case $L1$, the velocity profiles depend on both the SGS model and the smearing kernel size, indicating that the $\epsilon^t(\boldsymbol{x})$ and the $\epsilon^b(\boldsymbol{x})$ are qualitatively dominant errors. The velocity profiles from the iLES and WALE models are closer together. The SM

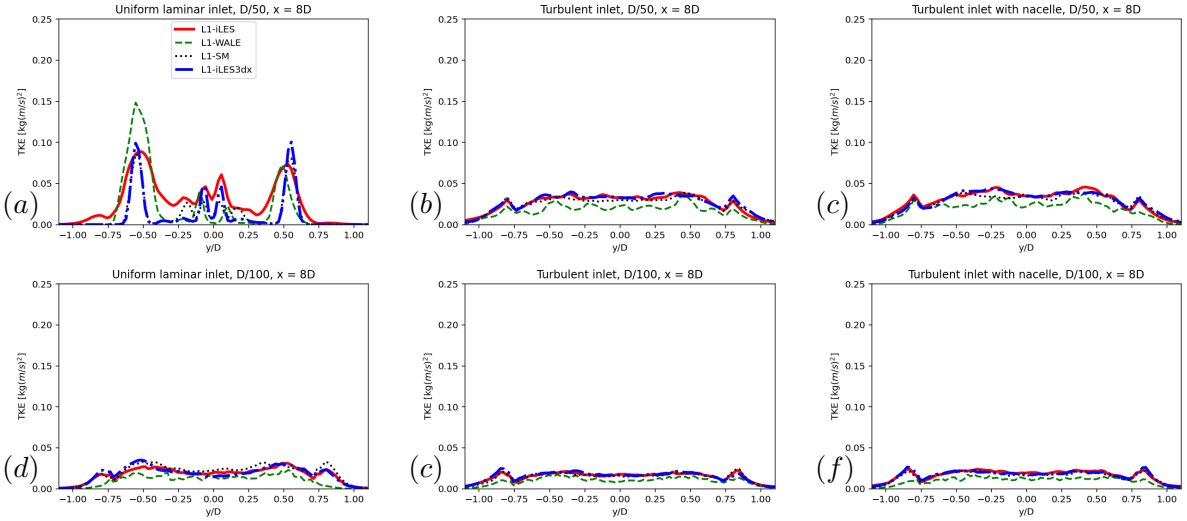

Figure 11. Time-averaged resolved TKE profiles downstream $8D$ wind turbine at $z = 1H$ under the uniform laminar (a) (d), the turbulent inlets (b) (e), and the turbulent inlets with nacelle (c) (f). The upper row is for coarse grid, and the bottom row is for fine grid.

and iLES with $\varepsilon = 3\Delta x$ provide the similar velocity profiles, and both show the a slower wake recovery, as illustrated in Figure 2. For case $L2$, the velocity profiles mainly depend on the smearing kernel size, which indicates the $\epsilon^b(\boldsymbol{x})$ is the qualitatively dominant error. For the left cases under a turbulent inlet, we observe the velocity profiles agree well with each other despite the varying SGS models, the grid resolution and the smearing kernel size.

Figure 11 presents the time-averaged resolved TKE profiles downstream $8D$ wind turbine at $z = 1H$. The resolved TKE profiles depend on both the SGS model and the smearing kernel size at a uniform laminar inlet, whereas at a turbulent inlet, they mainly depend on the SGS model. In particular, the WALE model produces smaller resolved TKE values in all cases with a turbulent inlet. We also observe that smaller TKE is resolved in the $T2$ and T_N2 cases with the fine grid than in the $T1$ and T_N1 cases with the coarse grid. Therefore, the WALE model resolves the TKE better under a coarse grid. For cases with the turbulent inlet, the dominant errors qualitatively are the numerical discretisation error $\epsilon^n(\boldsymbol{x})$, and the SGS modelling error $\epsilon^t(\boldsymbol{x})$.

5. Conclusion

In a Large Eddy Simulation (LES) of a wind turbine using the Actuator Line Method (ALM), the total numerical error is decomposed into three components: the numerical discretisation error, the Sub-grid Stress (SGS) modelling error, and the blade modelling error. This paper focuses on evaluating the dominant errors in ALM simulations of wind turbines, particularly the detailed comparisons between the implicit LES (iLES) and the explicit LES (eLES) models: Wall-adapting Local Eddy-viscosity (WALE) model and Smagorinsky model (SM).

For the total power coefficient and the aerodynamic loadings, the numerical discretisation error and the blade modelling error qualitatively dominate. Compared to the laminar inlet, the turbulent inlet causes larger fluctuations in the power coefficient and aerodynamic loadings. In the near-wake region, the velocity profile is insensitive to the SGS models, but depends on the smearing kernel size. This indicates that the blade modelling error qualitatively dominates. The numerical discretisation error and the SGS modelling error qualitatively dominate the performance of the resolved Turbulent Kinetic Energy (TKE). The blade modelling error

qualitatively dominates the power spectral density behaviour.

In the far-wake region, the blade modelling error and the SGS modelling error qualitatively dominate the time-averaged velocity performance under a laminar inlet. Under a turbulent inlet, however, the velocity profiles agree well with each other despite the varying SGS models, grid resolution, and smearing kernel size. For cases involving a turbulent inlet, the dominant errors in resolving the TKE qualitatively are the numerical discretisation error and the SGS modelling error. The WALE model gives a slightly better solution than the iLES and SM under the coarse grid.

In summary, our findings indicate that the explicit SGS model may not be necessary for predicting the total power coefficients and aerodynamic loadings. Under a turbulent inlet, the time-averaged velocity is insensitive to SGS models, whereas the WALE model with a coarse grid provides slightly better TKE resolution than the iLES and SM in the far-wake region. Subsequently, cases involving higher TI and length scales will be implemented to explore the feasibility of using iLES for ALM of wind turbine simulations.

Acknowledgments

CRV acknowledges the support of the UKRI, UK through his Future Leaders Fellowship MR/V02504X/1. QB. Li thanks the support of National Natural Science Foundation of China (12372218).

References

[1] Sorensen J N and Shen W Z 2002 Numerical modeling of wind turbine wakes *J. Fluids Eng.* **124** 393–399

[2] Zormpa M, Zilic de Arcos F, Chen X, Vogel C R and Willden R H 2025 The effect of flow sampling on the robustness of the actuator line method *Wind Energy* **28** e2965

[3] Manabe S, Smagorinsky J and Strickler R F 1965 Simulated climatology of a general circulation model with a hydrologic cycle *Monthly Weather Review* **93** 769–798

[4] Ducros F, Nicoud F and Poinsot T 1998 Wall-adapting local eddy-viscosity models for simulations in complex geometries *Numerical Methods for Fluid Dynamics VI* **6** 293–299

[5] Vreman A 2004 An eddy-viscosity subgrid-scale model for turbulent shear flow: Algebraic theory and applications *Physics of fluids* **16** 3670–3681

[6] Boris J P, Grinstein F F, Oran E S and Kolbe R L 1992 New insights into large eddy simulation *Fluid dynamics research* **10** 199

[7] Grinstein F F, Margolin L G and Rider W J 2007 *Implicit large eddy simulation* vol 10 (Cambridge university press, Cambridge)

[8] Cao G, Zhao W and Chen S 2022 Quantitative analysis on implicit large eddy simulation *Physics of Fluids* **34**

[9] Sarlak H, Meneveau C and Sørensen J N 2015 Role of subgrid-scale modeling in large eddy simulation of wind turbine wake interactions *Renewable Energy* **77** 386–399

[10] Huo P, Pan L, Wang Z, Cao G, Vogel C and Xu K 2025 Gpu-enabled high-order gas-kinetic scheme for actuator line model simulations of wind turbine wakes *Journal of Physics: Conference Series* vol 3016 (IOP Publishing) p 012017

[11] Krogstad P Å and Eriksen P E 2013 "blind test" calculations of the performance and wake development for a model wind turbine *Renewable energy* **50** 325–333

[12] Poletto R, Craft T and Revell A 2013 A new divergence free synthetic eddy method for the reproduction of inlet flow conditions for les *Flow, turbulence and combustion* **91** 519–539

[13] Zormpa M, Vogel C R and Willden R H 2026 Support structure modelling in actuator line method large eddy simulations of wind turbine wakes *Wind Energy* **29** e70077